Materials Today Energy 19 (2021) 100608

Contents lists available at ScienceDirect

Materials Today Energy

journal homepage: www.journals.elsevier.com/materials-today-energy/

# Design principles of MOF-related materials for highly stable metal anodes in secondary metal-based batteries

Y.Y. Hu [a], R.X. Han [a], L. Mei [a], J.L. Liu [a], J.C. Sun [b], K. Yang [a, **], J.W. Zhao [a, *]

[a] Henan Key Laboratory of Polyoxometalate Chemistry, College of Chemistry and Chemical Engineering, Henan University, Kaifeng, Henan, 475004, China
[b] School of Environment and Materials Engineering, Yantai University, Yantai, Shandong, 264005, China

ARTICLE INFO

*Article history:*
Received 2 November 2020
Received in revised form
25 November 2020
Accepted 26 November 2020
Available online 1 December 2020

*Keywords:*
Metal-organic frameworks
Metal anode protection
Metal dendrite
Volume expansion
Rechargeable battery

ABSTRACT

Secondary metal-based batteries (lithium metal batteries, sodium metal batteries, and zinc metal batteries) have appealed to increasing attention because of their high energy density. However, uncontrolled metal dendrite growth and infinite volume expansion can readily cause cycle performance deterioration and serious security concerns, which restrict their practical applications to a large extent. Recently, some coping strategies based on metal-organic frameworks (MOFs) and their derived materials have been proposed that demonstrate significant availability and great promise in constructing highly stable metal anodes. However, a relatively comprehensive overview that dissects the functions and applications of MOF-based materials based on the structure features of diverse MOFs and simultaneously covers all kinds of metal-based batteries is still absent. Here, according to recent achievements, we roundly summarize the design principles of MOF-related materials for stable metal (lithium, sodium, and zinc) anodes and further provide some suggestions for future developments. This review not only highlights important roles of MOF structures and diverse treatment strategies, but also endeavors to provide some enlightening guidance in designing dendrite-free metal-based batteries.

© 2020 Elsevier Ltd. All rights reserved.

## 1. Introduction

In the past two decades, developing clean sustainable energy storage and energy conversion technologies have captured increasing interest to meet environmental pollution and the forthcoming energy crisis [1–3]. Recently, metal-based batteries (e.g. lithium metal batteries, sodium metal batteries, and zinc metal batteries) have received major attraction because of their ultrahigh energy density [4–9]. However, owing to the high redox active metal surface and heterogeneous electrochemical deposition process, some serious problems such as metal dendrite, volume expansion, and electrode surface passivation occurred. These problems result in internal short-circuit to produce fearful security issue even though a solid electrolyte interface (SEI) formed by irreversible reaction between metal electrodes and electrolytes could suppress electrode surface passivation, dendrite, and corrosion [10]. For instance, in lithium-sulfur batteries, $LiNO_3$ as an electrolyte additive reacts with organic solvent and lithium bis(trifluoromethanesulfonyl)imide (LiTFSI) to form an SEI film, which restrains the lithium surface passivation and corrosion by polysulfides [11,12]. In aqueous zinc-based batteries, a water-in-salt electrolyte is used to create an insoluble SEI layer on the surface of the zinc anode to alleviate the corrosion of electrolyte [13]. However, it should be noted that the generated SEI layer fails to withstand the large volume expansion/shrinkage on account of poor mechanical properties, which results in cracking and exposing fresh metal surfaces, and then accompanying the generation of new SEI layer in the charge–discharge process, leading to the formation of heterogeneous and thick layer with poor ion conductivity [14–16]. Thus, electrochemical performances of metal-based batteries would undergo accelerated deterioration during cycling (Fig. 1). To cope with these problems, some functional materials (e.g. various nanocarbons, polymers, and metal nanoparticles) have been adopted to fabricate artificial SEI layers, gel or solid-state electrolytes, multifunctional separators, and advanced 3D anodes to stabilize various metal anodes [14,17,18].

Metal-organic frameworks (MOFs) are an emerging class of porous crystalline materials constructed by the self-assembly of metal ions or their clusters linked by multifunctional organic ligands, and carry high surface areas, large pore volumes, tunable

* Corresponding author.
** Corresponding author.
*E-mail address:* zhaojunwei@henu.edu.cn (J.W. Zhao).

https://doi.org/10.1016/j.mtener.2020.100608
2468-6069/© 2020 Elsevier Ltd. All rights reserved.

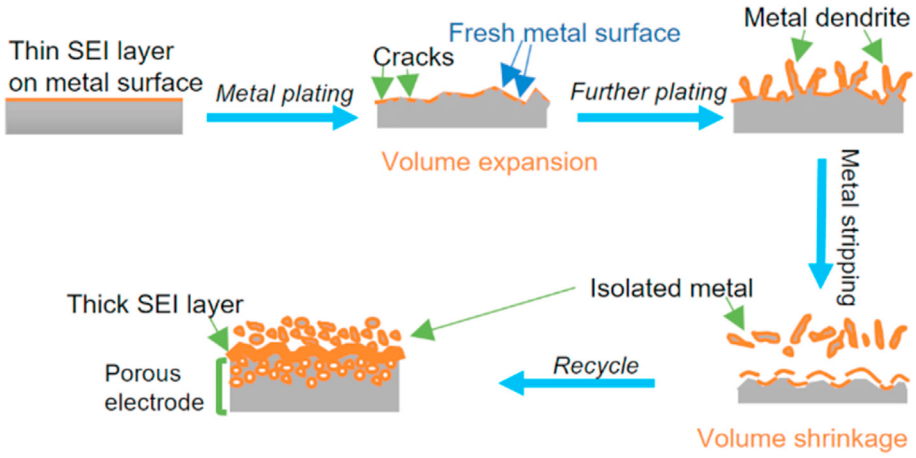


**Fig. 1.** Illustration of the SEI layer change on metal plating and stripping process.

pore sizes, distinctive characteristic features, and surface chemistry, which endow them with diverse and outstanding physiochemical properties. Over the past decades, approximately 70,000 MOFs have been manufactured and manifested broad and promising application prospects in proton conduction, catalysis, drug delivery, optoelectronics, and gas storage/separation [2,19–21]. In energy storage field, MOFs have been also used to multifunctional electrolytes or electrodes [22–25]. Besides, tremendous inherent advantages (structural diversity, functionality, and tailor ability) of MOFs can be used to improve ion conductivity and homogeneous deposition process of metal on the surface of metal electrodes. In this respect, some progresses on MOFs in inhibiting metal dendrite growth and withstanding volume changes have been reported. Developing MOF-related materials used for advanced energy storage systems has become a rapidly expanding and very prospective research area. To further promote the development of MOFs, numbers of excellent reviews that focused on the research of MOF materials in energy storage and conversion have been published recently [2,19,26]. Wang et al. have summarized recent advances about the protection of lithium metal anode and given reasonable predictions of future development trends and prospects in this field, in which the classification of MOF-based materials is based on application modes such as electrolytes, separators, and SEI films [27]. However, the applications of MOF-related materials in other burgeoning metal-based batteries (e.g. sodium metal batteries and zinc metal batteries) have less been involved. The design principles of MOF-related materials are still ambiguous. Hence, we provide an overall review on the applications of MOF-related materials in metal anode protection including lithium, sodium, and zinc anodes in secondary metal-based batteries, dissect functions, and applications of MOF-related materials based on the features of diverse MOFs and anticipate to provide some useful information and enlighten to further promote the development of MOF-related materials in next generation energy storage areas.

## 2. Recent achievements of MOF-related materials for metal anode protection

### 2.1. Metal lithium anodes

Metal lithium is a promising electrode material for manufacturing high energy density batteries because of its high theoretical specific capacity (3,860 mAh/g) and high negative potential (−3.040 V vs SHE) [28–30]. Developing metal lithium batteries has attracted great concern. Owing to the unstable metal lithium with uncontrollable dendrite growth and thick SEI film formation, recently, some treatment approaches have been developed to assuage these problems by constructing three-dimensional lithium anodes or anode protection layers and selecting appropriate electrolytes or electrolyte additives [31–44]. Thus, controlling uniform lithium nucleation, constructing homogeneous $Li^+$ transportation channels and creating stable interfaces between electrolytes and anodes enhance uniform lithium plating/stripping to realize stable electrochemical performance. To date, some versatile MOF-related materials applied to construct electrolytes separators, SEI layers, and anodes have been successfully used to inhibit lithium dendrite growth and mitigate the influence of volume changes during cycling. According to the features and functions of MOFs in ordered porous structure, center metal ions and organic ligands, we classified and summarized the recent achievements of MOF-related materials on lithium anode protection in the following discussion.

#### 2.1.1. Ordered porous structures

*2.1.1.1. Uniform ion channels.* MOFs possess various open porous structures and controllable ion transport channels to selectively guide homogeneous ion transport behavior and thus bring about dendrite-free metal surface. But the rigidity of MOFs can severely constrain some practical applications as flexible solid-state electrolytes (SSEs), separators, and high intensity SEI films. Hence, combination of polymers, one- or two-dimensional materials with MOFs can construct robust MOF-based gel electrolytes, SSEs, separators, as well as SEI films, which endow MOF-related materials with excellent mechanical properties to meet various requirements in physical variation. For instance, nano–MOF-199 (HKUST-1, formed by Cu(II) and benzene-1,3,5-tricarboxylate [BTC] ligands) with suitable $Li^+$ pathways and controllable particle sizes mixed with poly(vinylidene fluoride) (PVDF) binder was coated on metal lithium surface as an artificial SEI layer [45]. Galvanostatic cycling of lithium deposition and stripping by making use of MOF-199–coated Cu electrodes and symmetrical cells of different preloaded lithium electrodes demonstrated that nano–MOF-199 could stabilize the surface of metal lithium and relieve the formation of extra SEI layer. Zhang et al. used the rigid Zn–MOF sheet (synthesized by $Zn(NO_3)_2{\cdot}6H_2O$ and 2-methylimidazole on the surface of Cu foil) with good electrolyte wettability and abundant pore channels to effectively shield ions and hinder the anion migration, so as to enhance $Li^+$ migration behavior and inhibit Li dendrite growth. High-viscosity polyvinyl alcohol (PVA) cements MOFs to ameliorate the flexibility of Zn–MOF sheets and maintain

the high $Li^+$ conductivity in the layer (Fig. 2a). Under the protection of the Zn–MOF/PVA layer, the dendrite growth of Li anode was effectively inhibited, which resulted in the high coulombic efficiency (~97% over 250 cycles) at a current density of 3 mA/cm$^2$. Moreover, the flexible layer could efficiently bear the severe volume changes during continuous cycles to improve the stability of metal Li anode significantly [46]. A high porosity 3D lithium host with high ion conductivity and structure stability can uniformly distribute Li over a large-area surface, which may be probably a better strategy to control lithium dendrite growth and continuous volume variation. Thus, MOF-808 (prepared by trimesic acid and $ZrOCl_2 \cdot 8H_2O$) and PVDF slurry was used to decorate a 3D conductive scaffold (MOF@PVDF–HFP), in which the insulating coating layer favors to generate a dense and dendrite-free deposited layer with negligible electrode volume variation (<5% for 20 mAh/cm$^2$) [47]. Recently, a high porosity ZIF-8 (zinc 2-methylimidazolate) as a 'securer' showed the mechanical strength and porosity advantages of ZIF-8 in stabilizing Li anode [48].

Recent research results have demonstrated that some insoluble solid additives (e.g. LiF, $Li_3N$, $Al_2O_3$) have remarkable effects on resisting anode dendrite growth [49–51]. Highly porous graphitic carbon nitride (g-$C_3N_4$) mesoporous microspheres also facilitated the uniform lithium deposition on the anode substrate [54].

Introducing electrolyte additives to electrolyte is a simple and effective method to restrain the formation of dendrites and maintain the electrolyte stability [34,55,56]. Owing to the unique merits of porous MOFs, the researches on MOF-based electrolyte additives have also gained some progresses. For example, UiO-66 (zirconium 1,4-dicarboxybenzene), HKUST-1, and Al-based MIL-101–$NH_2$ (formed by $AlCl_3 \cdot 3H_2O$ and 2-aminoterephthalic acid) as electrolyte additives have positive effect on Li anode stability. The porous MOF additives with robustness and electrochemical stability could regulate the concentration of LiF in SEI, further restrained the undesired side reaction and homogenizing the $Li^+$ flux (Fig. 2b) [52].

*2.1.1.2. Controllable pore sizes.* Lithium–sulfur batteries may be the hopeful candidates for next-generation high energy density storage devices. However, poor electrochemical performances stemming from the serious polysulfide shuttle behavior and the generation of uncontrolled lithium dendrite heavily impede their industrial application [57–60]. Controllable porous MOFs bearing smaller pore size than soluble polysulfides ($S_n^{2-}$, $4 < n \leq 8$), acted as ion sieves, are able to deliver the extraordinary performance for suppressing the severe polysulfides migration [61–63]. On the basis of their merits, choosing suitable MOF material as lithium–sulfur battery separator to simultaneously suppress the polysulfide shuttle behavior of sulfur cathode and dendrite growth of lithium anode is considered to be a fruitful manipulating approach. Zhou et al. made use of a small porous HKUST-1 (pore size, 9 Å) and PVDF–HFP to prepare a novel separator to immobilize lithium polysulfides and maintain the unblocked $Li^+$ pathway (Fig. 2c) [53]. The highly uniform porous MOFs were conducive to homogenize $Li^+$ flux thereby maintain a flat surface at an ultrahigh current density of 10 mA/cm$^2$. As a result, the lithium–sulfur battery exhibits superior long life span and capacity retention. Similarly, a polyolefin separator modified by MIL-125(Ti) ($Ti_8O_8(OH)_4(BDC)_6$, BDC = 1,4-benzene dicarboxylate) coating layer also proves the superior ability in regulating polysulfide shuttle and Li dendrite growth [64].

Compared with 3D MOFs, 2D MOF nanosheets with larger aspect ratio facilitate to raise both $Li^+$ transference number and mechanical strength of MOF-based composite materials [65]. Recently, Wang et al. firstly introduced a novel 2D filler (constructed from Ni and aromatic benzenedicarboxylic acid $(BDC)^{2-}$ ligands) into polyethylene oxide (PEO)-based composite electrolyte. The ultrathin nanosheet with larger surface engineers shorter and continuous ion transfer path at the increased PEO/MOF interfaces. The central Ni ions possess smaller coordination numbers could give rise to stronger interaction with PEO [66]. Inspired by these merits, Guo' group reported a 2D MOF-Co (Co single atom array mimic on ultrathin MOF nanosheets) separator to homogenize $Li^+$ flux and suppress 'polysulfide shuttle' [67]. In the separator, Co atoms coordinated with O atoms are exposed on the surface of MOF to uniform $Li^+$ flux by the strong interaction between $Li^+$ and O atoms at the anode and separator interphase. In addition, Co single atoms that provide Lewis acid–base interaction effectively immobile polysulfides. As a result, the bifunctional separator enables a safe and long-term lithium–sulfur battery.

### 2.1.2. MOFs as anion hosts

As well known, owing to the presence of Lewis acidic sites of highly dispersed and plentiful transition-metal cations in the structures, porous MOF hosts have the ability to encage functional

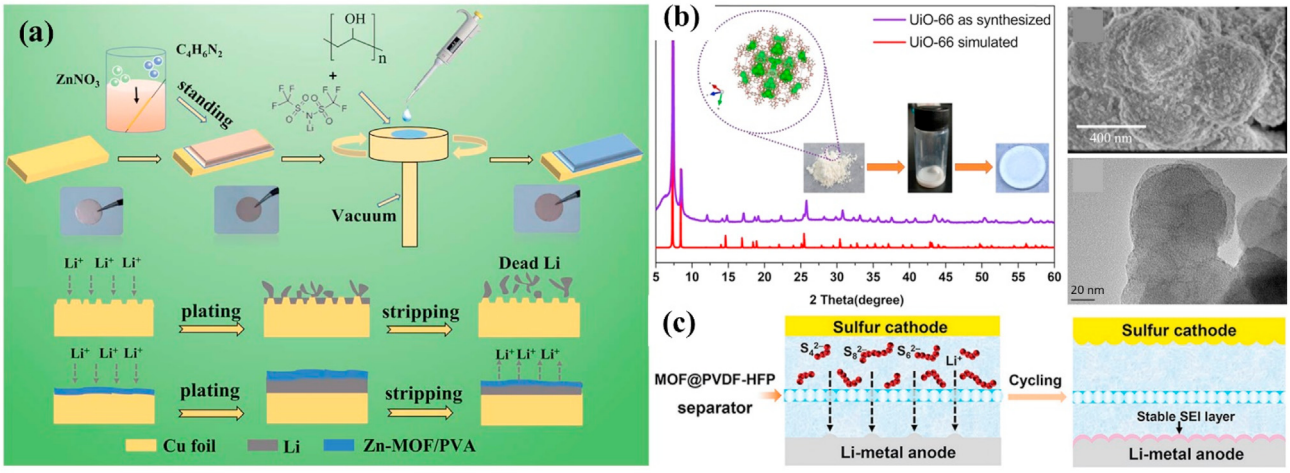


**Fig. 2.** The functions of ordered porous structures in MOFs. (a) Fabrication process of Zn–MOF/PVA layer and schematic illustration of lithium plating/stripping behavior on different Cu foil. Reprinted with permission from Ref. [46]. (b) Schematic illustration of $LiPF_6$ electrolyte with UiO-66–Li additive and the corresponding XRD pattern and morphology of UiO-66. Reprinted with permission from Ref. [52]. (c) Schematic illustration for lithium–sulfur batteries with MOF@PVDF–HFP separator. Reprinted with permission from Ref. [53].

anions in the pores, so as to improve ion transport behavior [36,68]. Recently, many efforts have been devoted to design novel MOF-related materials by characteristic interactions of metal cations with ionic liquids (ILs) or electrolyte anions.

*2.1.2.1. ILs guests.* The typical MOF-based ionogels generally consist of common characteristics of ILs and MOFs and exhibit high ion conductivity, good physical and chemical stability [36]. A electrochemically stable IL-impregnated MOF-525 (built by $Zr_6(IV)O_4(OH)_4$ clusters and [5,10,15,20-tetrakis(4-carboxyphenyl) porphyrin]Cu(II) organic linkers) (Li–IL@MOF-525) was prepared by Pan et al., which displays a high room-temperature ionic conductivity ($3.0 \times 10^{-4}$ S/cm) and $Li^+$ transference number (0.36) [38]. The Li plating/stripping experiments show small polarization voltages and stable cycling over 1,000 h at 0.05 and 0.2 mA/cm$^2$, indicating the stable interface between the Li–IL@MOF electrolyte and metal lithium anode. In addition, they adopted different sized Li–IL@UiO-66 nanoparticles to investigate the size effect for lithium stripping/plating process [39]. Owing to higher packing density, the synergistic effect of hybrid nanoparticles [larger nanoparticles (~200 nm) can suppress Li dendrite growth, whereas smaller nanoparticles (~20 nm) make for the better contact with lithium] demonstrates superior suppressing dendrite growth ability. Moreover, Pan et al. adopted the mixture of Li–IL@MOF and $Li_7La_3Zr_2O_{12}$ (LLZO) to elevate the $Li^+$ ion conductivity and withstand the Li dendrite growth (Fig. 3a). In the composite material, nanosized Li–IL@MOF particles are filled into the interspace of LLZO particles, which significantly enhance $Li^+$ ion transportation kinetics. Therefore, the hybrid SSE displays a high ionic conductivity of $1.0 \times 10^{-4}$ S/cm and a wide electrochemical stability window of 5.2 V at ambient temperature [44]. In addition, Guo et al. used UiO-66 adsorbed Li-containing IL EMIM–TFSI [1-ethyl-3-methylimidazolium bis((trifluoromethyl)sulfonyl) imide)] as a filler to strengthen PEO electrolyte [69]. The filler could enhance ionic conductivity ($1.3 \times 10^{-4}$ S/cm at 30 °C) of SSEs and suppress crystallinity of PEO. This work provides a new approach for the application of MOF materials in fabricating high-performance solid electrolytes. Recently, Mai et al. reported an ultraviolet cross-linked solid electrolyte that modified by ZIF-based ionic conductor (prepared by 1-ethyl-3-methylimidazolium-bis(trifluoromethyl sulfonyl) imide (EMIM-TFSI) guest embedded ZIF-8 host). In this composite electrolyte, the ultraviolet irradiation formed amorphous polymer region and constructed solid–liquid transport interface between ZIF-based ionic conductor and polymer chains delivers fast ion transport and excellent Li|Li compatibility cycle on 1,040 h [70].

By virtue of low melting point, negligible volatility and nonflammability of ILs, the good thermal stable IL@MOF served as quasi-solid-state electrolyte maintains high ionic conductivity at a wide temperature range and thus deliver high electrochemical performance [37,71,72]. Fujie et al. reported the first example of EMI–TFSA@ZIF-8 by incorporating IL [EMI–TFSA (1-ethyl-3-methylimidazolium bis (trifluoromethylsulfonyl) amide)] into ZIF-8 [$(Zn(MeIM)_2$, H(MeIM) = 2-methylimidazole], which exhibits nonfreezing effect at 123 K and maintains the high ionic conductivity and excellent electrochemical performance [37]. High-temperature lithium metal batteries have displayed great potentials in electronic instruments in extreme environments, such as ultra-deep and deep ground detection, space exploration, and underground heat source development. However, not only the violent evaporation of the electrolyte solvents, but also the increased reaction activity of the metal lithium anode with electrolytes at elevated temperature would engender safety hazard and lower cycling performance [40]. To avoid the serious hazard, Chen's group mixed an IL electrolyte ILE, a mixture of *N*-propyl-*N*-methylpyrrolidinium bis(trifluoromethylsulfonyl) imide ([Py13][TFSI]) and lithium bis(trifluoromethylsulfonyl)imide (LiTFSI) with zeolitic imidazolate framework–67 (ZIF-67) particles via simple ball-

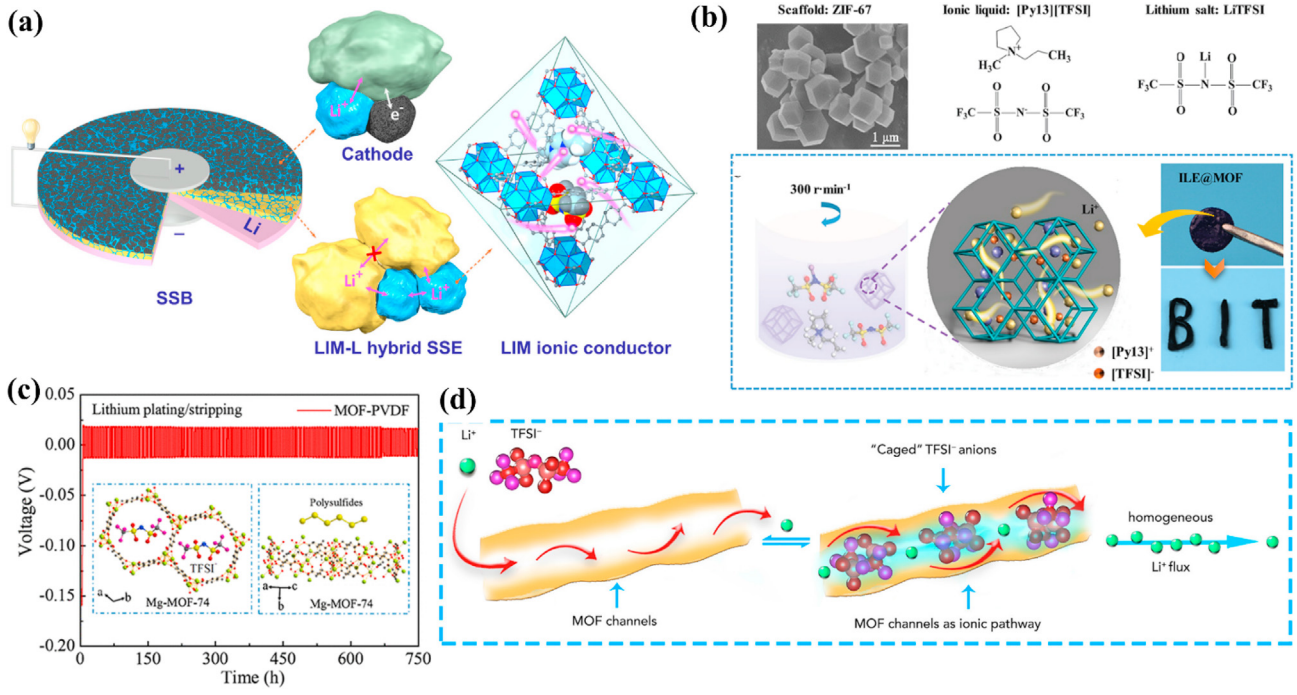


**Fig. 3.** Research progresses of MOF-based anion hosts. (a) The architecture of the hybrid SSE with Li–IL@MOF and LLZO as well as its migration mechanism. Reprinted with permission from Ref. [44]. (b) Photographs of ILE@MOF materials and the schematic illustration of its synthetic method and $Li^+$ transport paths. Reprinted with permission from Ref. [41]. (c) Schematic illustration of Mg–MOF-74 containing $TFSI^-$ and the corresponding voltage profile of Li/MOF–PVDF/Li cell. Reprinted with permission from Ref. [73]. (d) Schematic of the $Li^+$ migration in MOF host. Reprinted with permission from Ref. [75].

milling to gain an ILE@MOF iongel (Fig. 3b) [41]. The encapsulated ILE still retains its dynamic mobility and shows high ion conductivity because of strong interaction between $TFSI^-$ anions and metal cations of MOF to improve $Li^+$ mobility. Benefit from the superior merits of MOF-based ionogels, the metal lithium stability is effectively improved by forming a stable particle-rich coating over the anode to protect the lithium anode at high temperature. It is obvious that the Li metal with this new electrolyte demonstrates a stable plating/stripping process over 1,200 h at a high temperature of 150 °C and a current density of 0.5 mA/cm$^2$.

*2.1.2.2. Electrolyte guests.* Guest PVDF with the large dielectric constant ($\varepsilon = 8.4$) and strong C–F bonds is still hampered by the poor interfacial stability with the metal lithium anode. To address these issues, PVDF-based gel polymer electrolyte (GPE) that was modified by Mg–MOF-74 (synthesized by ($Mg_2O_2(CO_2)_2$) and 2,5-dioxido-1,4-benzenedicarboxylate) was proposed. Here, the obtained MOF–PVDF GPE with abundant Lewis acid sites has the appropriate pore size (10.2 Å) to encage $TFSI^-$ ions, which facilitates the homogeneous lithium deposition (Fig. 3c) [73].

Inserting fillers with Lewis acid surfaces into polymer electrolytes can enhance the ionic conductivity and stabilize the electrolyte/lithium interfaces effectively, which are limited by the nature of fillers and their surface states [74]. A nickel-1,3,5-benzene tricarboxylate MOF ($Ni_3$–$(BTC)_2$–MOF) together with LiTFSI and PEO were used to form a composite solid-state electrolyte, which exhibits a high $Li^+$ transference number, excellent mechanical and thermal properties. Organic functional groups of $Ni_3$–$(BTC)_2$–MOF enhance the compatibility with polymer segments and thus improve interfacial properties and ionic conductivity ($1.4 \times 10^{-4}$ S/cm and $4.5 \times 10^{-3}$ S/cm at 30 and 70 °C) [38]. Furthermore, the composite electrolyte membrane shows the excellent performance in inhibiting lithium dendrite growth. Zhou et al. added porous HKUST-1 (pore size: 8 Å) into the liquid electrolyte, which could act as a host to cage electrolyte anions ($TFSI^-$, length: 7.9 Å). Moreover, the density functional theory (DFT) calculations were applied to illustrate the migration barrier while $TFSI^-$ anions pass through porous MOF skeletons (Fig. 3d). A preference of $Li^+$ migration behavior was also further testified by the DFT-based molecular dynamics simulation, which is conducive to uniformize $Li^+$ flux [75]. The MOF-modified electrolyte achieved a high $Li^+$ transference number and facilitated a homogeneous $Li^+$ plating/stripping process at a high current density. Dunn et al. reported a flexible PTFE-based pseudo-SSE with biomimetic ionic channels by complexing the $ClO_4^-$ anions to the open metal sites of HKUST-1, which enables transportation of $Li^+$ ions with low activation energy [76]. Then, the SSE affords a high ionic conductivity with fast $Li^+$ transport kinetics.

Other guests are also encaged into MOF's porous structures to get the multifunctional MOFs. For instance, the dual lithiophilic structure of electron-conductive Ag nanoparticles permeating polar MOF (HKUST-1) (Ag@HKUST-1) could reduce the overpotential of lithium nucleation to nearly zero [77].

Highly conductive Ag seeds hoist the electron transfer kinetics of MOFs, and the large surface area of HKUST-1 cuts down the local current density and provides abundant space for the initial Li nucleation.

### 2.1.3. Functional organic ligands

Organic ligands in MOFs provide extra opportunities to introduce functional groups, which endow MOFs with versatility. Thomas's work demonstrated that magnesium-1,4-benzenedicarboxylic acid (Mg–TPA) offered higher ionic conductivity than that of Mg–TMA on account of the less surface charges of TPA to fasten $Li^+$ migration within the electrolyte [78]. Besides, to modify MOFs with extra capability, the functionalized organic ligands by various polar groups were also used to develop novel separators or electrolytes in recent achievements.

*2.1.3.1. Organic ligands functionalized by $-NH_2$.* Sun and Guo used $NH_2$–UiO-66 as a filler to optimize the PEO/LiTFSI matrix and gained the anion-immobilized polymer electrolyte [79]. As shown in Fig. 4a, UiO-66 can immobilize anions and direct uniform $Li^+$ deposition. Owing to the high specific surface area and $-NH_2$ group in UiO-66, the polymer electrolyte reveals strong anion absorption, leading to a high $Li^+$ transference number of 0.72. Moreover, the ionic conductivity (from $3.9 \times 10^{-6}$ S/cm to $3.1 \times 10^{-5}$ S/cm) and electrochemical stability window (4.97 V) are all enhanced. In addition, a functional glass fiber separator via *in-situ* growing $NH_2$–UiO-66 on the glass fiber was designed to effectively alleviate $Li^+$ transport limitation and concentration polarization [80]. The substantially improved $Li^+$ transference number (0.67) produces a smooth lithium surface on cycling because of the anchored anions. To integrate high ionic conductivity with high mechanical property in polymer electrolyte, $NH_2$–UiO-66 could be further grafted by methacrylic anhydride to synthesize a chemically cross-linked MOF-based polymer electrolyte. The material effectively alleviates the volume variation as well as dendrite growth of lithium and maintains the excellent electrochemical stability of batteries [81]. The reported separators modified by inorganic compounds (e.g. $Al_2O_3$ [82,83], $TiO_2$ [84,85], or BN [86]) hinder $Li^+$ diffusion in spite of their high mechanical strength, because of the absence of chemical interactions between inorganic compounds and ions in the electrolytes [87–90]. Differently, MOFs as ion sieves offer suitable 3D open channels and organic functional groups to influence the migration of $Li^+$ via chemical interactions. Wang et al. coated a titanium-based $NH_2$–MIL-125(Ti) (prepared by $Ti_8O_8(OH)_4$ nodes and 2-aminobenzene-1,4-dicarboxylate linkers) on a commercial polypropylene (PP) separator to enable stable lithium surface with low electrochemical resistance even at a long-term plating/stripping process (Fig. 4b) [91]. It has proved that amine groups in $NH_2$–MIL-125(Ti) play an important role in increasing $Li^+$ transference number and inducing uniform lithium nucleation and deposition.

*2.1.3.2. Organic ligands functionalized by $-SO_3^-$.* In lithium–sulfur batteries, introducing anion groups into cathodes or separators to suppress polysulfides by electrostatic repulsion interaction are identified as effective strategies [92–95]. Park's group synthesized a sulfonated UiO-66 (UiO-66–S) to develop a MOF/Nafion hybrid separator, in which 'polysulfide shuttle' was effectively mitigated on account of the electrostatic repulsion of $-SO_3^-$ from UiO-66–S and Nafion, and the adequate molecular sieving of the smaller pore size of UiO-66 (Fig. 4c). After cycling, the functional separator contributed to deliver a dendrite-free metal lithium surface by means of UiO-66–S/Nafion hybrid coating [96]. In addition, a UiO-66–S derived solid electrolyte has been also developed, which exhibits high ionic conductivity, polysulfide-suppression capability, and good lithium anode stability [99].

*2.1.3.3. Organic ligands functionalized by large anionic groups.* Recently, single-ion conductive electrolytes have drawn considerable attention because of their unique ion transference number [100,101]. Kang and Su proposed a post-synthetic modification method to gain an MOF-based single-ion conducting electrolyte by anchoring a large anionic group on the skeleton of $NH_2$–UiO-66 via covalently coordination between trifluoromethanesulfonyl group and amino groups. As displayed in Fig. 4d, the preeminent single-ion conductive electrolyte demonstrates a high ion conductivity ($2.07 \times 10^{-4}$ S/cm at 25 °C) and $Li^+$ transference number (0.84) and

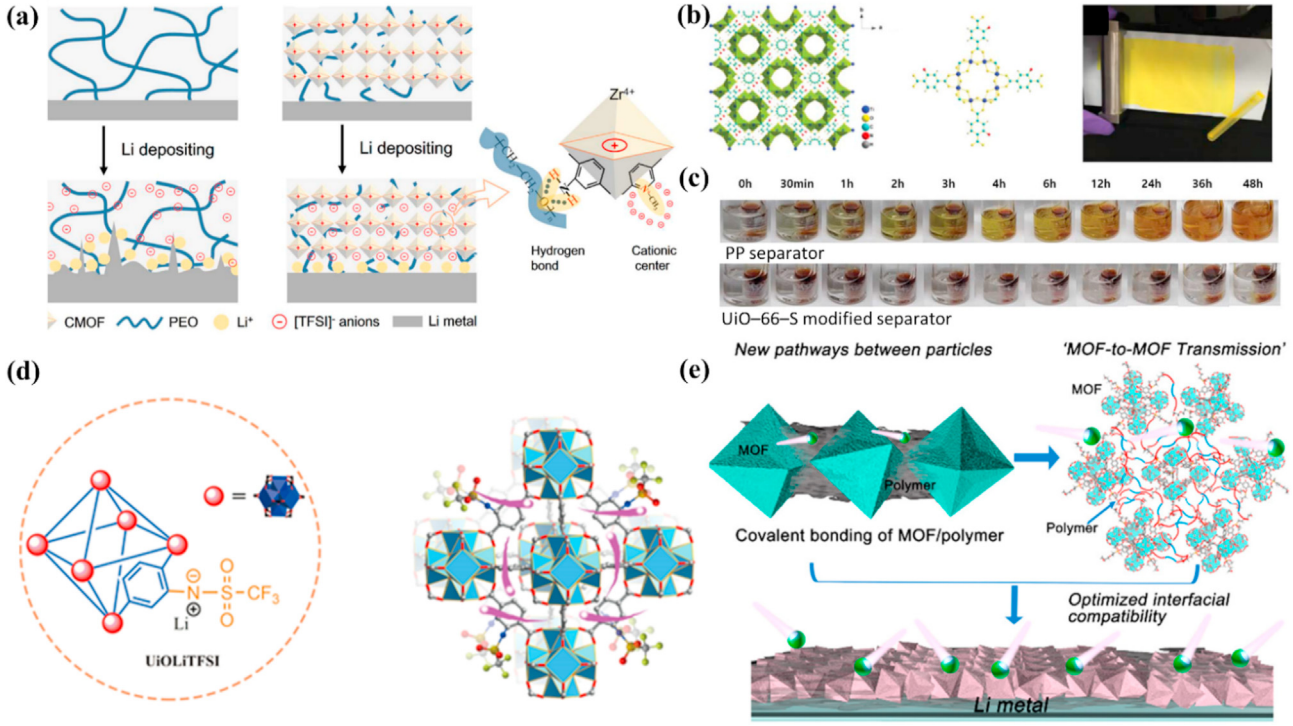


**Fig. 4.** Functional organic ligands of MOFs for stable Li anodes. (a) Schematic view of lithium deposition with PEO(LiTFSI) electrolyte (left) and anion-immobilized PEO@CMOF electrolyte (right). Reprinted with permission from Ref. [79]. (b) Illustration of $NH_2$—MIL-125(Ti)—decorated PP separator. Reprinted with permission from Ref. [91]. (c) Polysulfides diffusion tests of PP and UiO-66—S modified separators at different time. Reprinted with permission from Ref. [96]. (d) Schematic illustrations of MOF-based single-ion conducting solid state electrolytes and the corresponding rate performance of solid-state lithium metal batteries. Reprinted with permission from Ref. [97]. (e) Illustration of the structure and function of covalent bonding of MOF/polymer. Reprinted with permission from Ref. [98].

can effectively inhibit the formation of lithium dendrite when it was used as an SSE, which is conducive to gain solid-state lithium metal batteries with outstanding rate performance and cyclic stability [97].

In addition to versatile MOFs (functionalized by $-NH_2$, $-SO_3^-$, and large anionic groups) as mentioned earlier, the —COOH and —OH groups decorating MOFs have played the key role in optimizing interfaces between MOF crystals, enhancing ion conductivity, and improving the interfacial compatibility [102]. To improve interfacial compatibility of MOF-based solid electrolytes, building ion channels between MOF crystals is very necessary. Hence, MOF-CN that was synthesized by grafting 3-glycidoxypropyltrimethoxysilane (γ-GPS) onto UiO-66-2OH reacted with poly(ethylene glycol) diglycidyl ether and diaminopoly(propylene glycol) to form the covalent bonding interactions of MOF/polymer material (Fig. 4e) [98]. Abundant ion transport pathways at interfaces realized MOF-to-MOF ion transport and enhanced the interfacial compatibility. As a result, MOF/polymer material as a solid electrolyte presents the high ion conductivity, high $Li^+$ transference number, and stable Li plating/stripping behavior. Moreover, the evaluation of Zn|Zn symmetric cells with the solid electrolyte have also demonstrated that the as-obtained MOF/polymer electrolyte can effectively suppress Zn dendrite formation.

### 2.1.4. MOF-derived porous matrixes with uniform nucleation seeds

Pre-planting nucleation seeds is a useful approach to control the nucleation and lithium dendrite growth [7,103—105]. Besides, conductive 3D porous nanomaterials decrease effective current densities of electrodes, avoid the uneven charge accumulation, and resist infinite volume change [103,106—111]. Therefore, exploring a 3D lithiophilic host with homogeneous nucleation seeds is an ideal strategy to stabilize metal anodes. Yang et al. indicated that the carbonized Zn-based MOFs (ZIF-8) was an ideal 3D lithiophilic host, which could be used to fabricate the uniform lithium-carbonized MOF (Li—cMOF) hybrid material by facile molten lithium infusion method (Fig. 5a and b) [112]. In the hybrid material, uniformly distributed Zn clusters acted as preplanted nucleation seeds to induce uniform lithium deposition. Meanwhile, the obtained 3D conductive structure enables the uniform lithium plating/stripping by homogenizing the distribution of electric field and $Li^+$ flux on the surface of hybrid lithium anode. Hence, the hybrid lithium anode shows excellent high electrochemical stability and a long cycle life. This discovery offers a new opportunity for exploring stable Li anode based on diversiform MOF materials.

Similarly, a lithiophilic ZnO/carbon framework with abundant carbonyl and nitrogen-containing surface groups and ZnO sites was formed by pyrolysis of ZIF-8. The porous and lithiophilic ZnO/carbon scaffold effectively mitigates the volume change and lithium dendrite growth, which significantly enhances the stability of lithium anode [115]. Recently, Xia and Wang carbonized HKUST-1 to prepare nano-Cu in-situ embedded porous carbon material, and confirmed that the formed $CuC_x$ at the interface acting as lithiophilic sites to regulate lithium nucleation and deposition process. $Al_2O_3$ seeds even-distributed mesoporous carbon (derived from Al(OH)(1,4-naphthalenedicarboxylic acid)·$2H_2O$) as a host also showcased excellent performance in decreasing lithium nucleation overpotential and then homogenizing lithium deposition [116]. Moreover, CuO [117], $TiO_2$ [118], $Cu_{1.8}Se$ [119], $ZnCo_2O_4$/ZnO [120], and a hierarchical heterostructure with ZnO [121] also demonstrated good performance in regulating lithium nucleation and homogeneous $Li^+$ flux. Generally, integrating 3D host with isolated

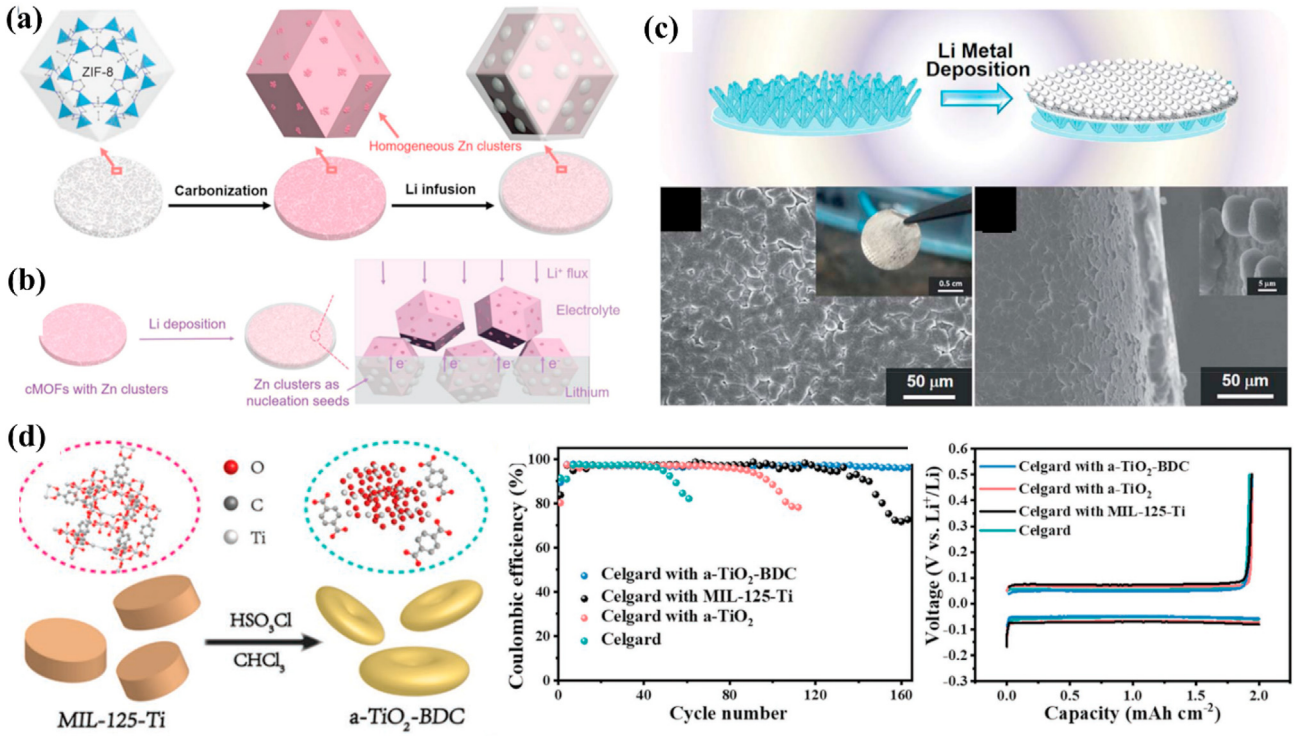


**Fig. 5.** Application strategies of MOF-derived materials. (a) Schematic illustration of the fabrication process of Li–cMOFs and (b) Lithium deposition behavior of cMOFs film with Zn clusters. Reprinted with permission from Ref. [112]. (c) Schematic illustration of lithium deposition on the NC/Cu electrode and SEM morphologies of the surface and cross-section of the Li–NC/Cu anode. Reprinted with permission from Ref. [113]. (d) Chemical reaction from MIL-125–Ti to a-$TiO_2$–BDC and the electrochemical tests of Li//Cu cells with different separators at 2 mA/cm$^2$ and mAh/cm$^2$. Reprinted with permission from Ref. [114].

Cu current collector could cause large polarization. Exploring a facile and scalable strategy to engineer a free-standing 3D anode host is significant for uniform lithium deposition. Recently, Ming et al. developed the integrated lithiophilic nitrogen–carbon anchored Cu nanorod arrays (NC/Cu) to facilitate homogeneous lithium deposition (Fig. 5c) [113]. Benefiting from the unique 3D structure and heteroatom compositions, the NC/Cu arrays that afford fast electron transport path, uniform $Li^+$ migration channel, and abundant space exhibit much lower interfacial resistance and more stable lithium anode surface. Recently, Fan' group also verified the similar design principle of a dendrite-free Li metal anode by a carbonized Co-ZIF (Co-based zeolitic imidazolate framework) nanorod arrays modified with carbon cloth or carbonized ZIF-67 with Co nanoparticles dispersed *N*-graphene to construct lithiophilic surface, buffer the volume change, and ensure homogenous Li nucleation [122].

Owing to designability in porous structures and chemical compositions, MOFs exhibit good performance in tuning $Li^+$ plating/stripping behavior. However, the efficiency and stability of the achieved metal Li electrodes for practical applications are still insufficient. Recently, a new material derived from decomposing MOF (MIL-125–Ti) into intimately mixed amorphous titanium dioxide and crystalline BDC, denoted as a-$TiO_2$–BDC, demonstrated better capability in suppressing Li dendrite growth than the oxide alone, the organic component alone, and the parent MOF, which illustrated that the material induced the formation of a moderate SEI layer with well mechanically flexible and ionic-conductivity to stabilize Li anode and block polysulfides (Fig. 5d) [114]. These achievements afford some new perspectives for exploring novel and effective MOF-related materials to regulate the metal ion stripping/plating behavior.

### 2.2. Metal sodium anodes

Metal sodium batteries have been considered as one of the prospective alternatives for electric vehicles and power grids, thanks to the low cost and extensive sodium resources [14,124–126]. Analogously, metal sodium anodes are also subjected to uncontrollable dendrite growth and infinite volume change in plating/stripping process [4,127–132]. Therefore, some effective approaches for metal lithium anode protection may be enlightening for restraining sodium dendrite growth. Inspired by this, Chen et al. used the artificial SEI film (a coating layer of nano–MOF-199 and PVDF) of metal lithium anodes to investigate the suppression ability of sodium dendrite [45,133]. Comparisons of the coulombic efficiency and SEM images of pristine Cu and MOF-199–coated Cu electrodes at a current density of 1 mA/cm$^2$ with a sodium deposition amount of 1 mAh/cm$^2$ indicate that the MOF-199 layer homogenize $Na^+$ ion concentration resulting in a stable metal sodium anode (Fig. 6a).

Owing to the definite solubility of main group II metal (Be, Mg, and Ba) in metal sodium, these metals can work as uniformly distributed nucleation seeds for guiding the homogeneous growth and deposition of metal sodium on the metal Be, Mg, and Ba substrates [105]. Hence, the nucleation barriers of sodium on the metal Be, Mg, and Ba substrates were investigated by Yang's group, demonstrating that the main group II metals indeed decrease the nucleation barriers of sodium and guide the parallel growth of sodium. Inspired by this discovery, an efficient strategy of carbonizing Mg-based MOF-74 to control deposition of sodium was put forward (Fig. 6b), where resulting Mg clusters homogeneously disperse in the obtained 3D hierarchical structure, which favors to eliminate sodium nucleation barriers, leading to the uniform

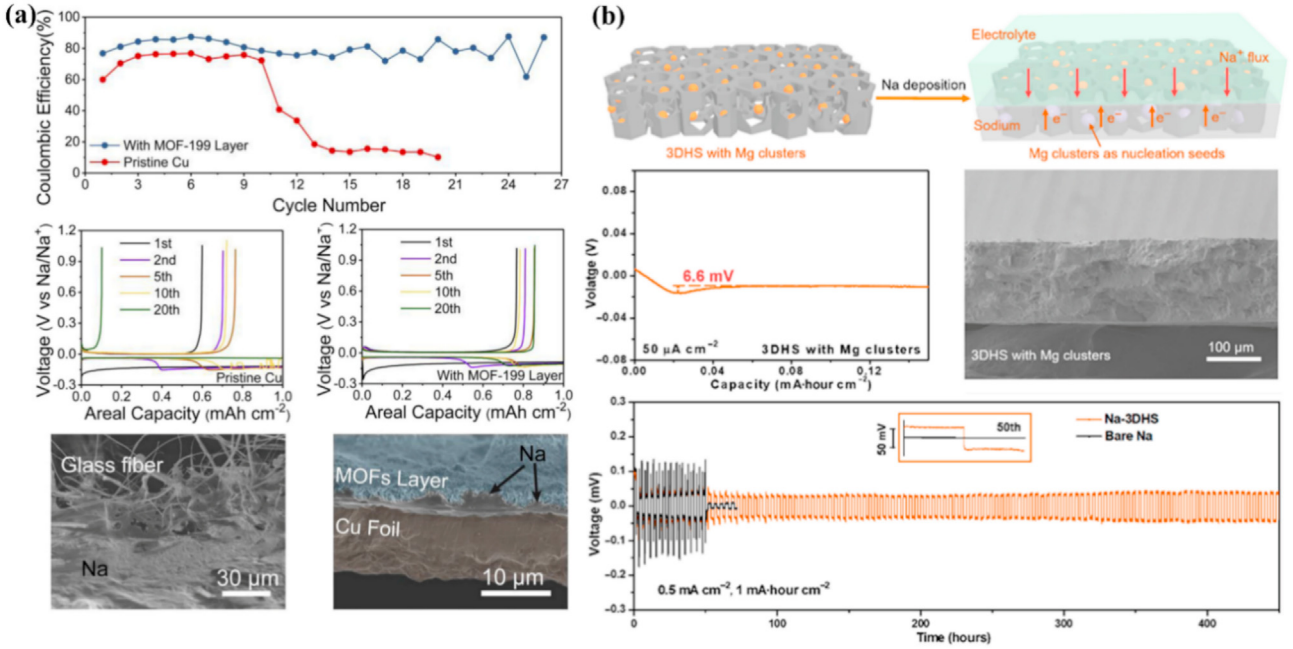


**Fig. 6.** Protection strategies of metal sodium anodes. (a) Coulombic efficiency of pristine Cu and MOF-199–coated Cu electrodes and the corresponding SEM morphologies of sodium anodes. Reprinted with permission from Ref. [45]. (b) Schematic illustration of controllable nucleation and growth of sodium in the carbonizing Mg-based MOF-74, SEM images, and cycling stabilities of sodium anode with and without the 3D materials. Reprinted with permission from Ref. [123].

sodium deposition [123]. Kim' group reported defect engineering and mesoporous carbon nanofibers derived from Zn, Ni bimetallic MOF, which possess uniform Na nucleation sites and functional groups (N, O) to reduce the adsorption energy barrier of Na and ameliorate Na deposition behavior [134]. Beyond that, a porous nitrogen-anchored carbon rhombic dodecahedron embedded with sodiophilic Co sites can also boost uniform sodium nucleation and deposition [135]. So far, the investigations on applying MOF-related materials to inhibiting sodium dendrite growth are still few. The summarization of lithium and sodium anode protection provides some beneficial assistances and enlightenments for developing efficient strategies to solve sodium dendrite and fabricate high stable metal Na anode via designing novel electrolytes, separators, SEI layers, as well as anode structures.

### 2.3. Metal zinc anodes

In comparison with $Li^+$, $Na^+$, and $K^+$ ion batteries [17,136,137], rechargeable aqueous zinc-ion batteries (ZIBs) using metal zinc anode reveals conspicuous advantages in safety and cost because of the abundant sources, low toxicity, low redox potential (−0.76 V vs SHE), and easy processing of metal zinc [6,138–141]. Recently, the researches on aqueous ZIBs have been focused on exploring pre-eminent $Zn^{2+}$ host materials and stable electrolytes [142–145]. Although electrochemical performances of some novel ZIBs have been greatly enhanced, the metal zinc anode dendrite, corrosion, and passivation seriously influence their applications [137]. The Zn nucleation occurs at a high Zn concentration at the beginning, and then the Zn deposition selectively proceeds at the exist crystals nucleus area to reduce the surface energy. As a consequence, the sustained growth of Zn nucleation would form the harsh dendrite, which is similar to the formation of Li and Na dendrites. Differently, owing to the narrow electrochemical stability window (1.23 V) of aqueous electrolyte, Zn anodes undergo the diverse corrosion and passivation process. On discharging, the side reaction of $H_2$ evolution increases the concentration of $OH^-$ ions. Meanwhile, Zn foil strips and then dissolves into the liquid electrolyte thereby form hydroxides and zincates byproducts, which would passivate the fresh Zn surface. The irreversible Zn corrosion and passivation destroy the cyclability of energy storage system with finite electrolyte (Fig. 7a) [137,149]. Therefore, continuously exploiting practical zinc anodes with stable and long life cyclability remains a rigorous challenge. Great efforts have been dedicated to fabricating artificial SEI films by using various nanomaterials and constructing 3D conductive zinc anodes by using carbon cloth, graphite felt wafer, and porous copper skeleton [15,17,150]. For example, Archer et al. reported a reversible epitaxial electrodeposition strategy to effectively drive deposition of Zn, which affords a general pathway toward high reversible energy-dense batteries [151].

#### 2.3.1. Ordered porous structures

As the versatile materials, the MOF-related materials were also selected to explore $Zn^{2+}$ diffusion kinetics and zinc plating/stripping behaviors. A single-ion $Zn^{2+}$ SSE was prepared by a post-synthetic modified Zn–MOF-808 ($Zr_6O_4(OH)_4(OH)_{12}Zn_3(BTC)_2$) and manifested high conductivity ($2.1 \times 10^{-4}$ S/cm) at 30 °C and high $Zn^{2+}$ transference number (0.93) [152]. It is extremely apparent that the nano-wetted Zn/SSE interface restricts the transport of $Zn(H_2O)_6^{2+}$ and guides zinc plating/stripping process.

Unlike non-aqueous alkali metal batteries, because of the absence of SEI films, poorly wetting effect of aqueous electrolyte on the zinc anode can cause high zinc plating/stripping polarization. Hence, using an artificial SEI to improve wetting effect is an efficient method for a well-contacted interface. For instance, Pan et al. firstly reported a simple coating method to construct a thin zincophilic interface by PVDF binder and hydrophilic nano-MOF (UiO-66) [146]. It can be verified that the MOF–PVDF–coated zinc surface in aqueous electrolyte presents a smaller contact angle and obviously decreases charge-transfer resistance as well as zinc nucleation over potential. Thus, the stable and dendrite-free zinc plating/stripping cycling performance and improved rate performance for the aqueous Zn/$MnO_2$ battery with MOF–PVDF–coated zinc anode

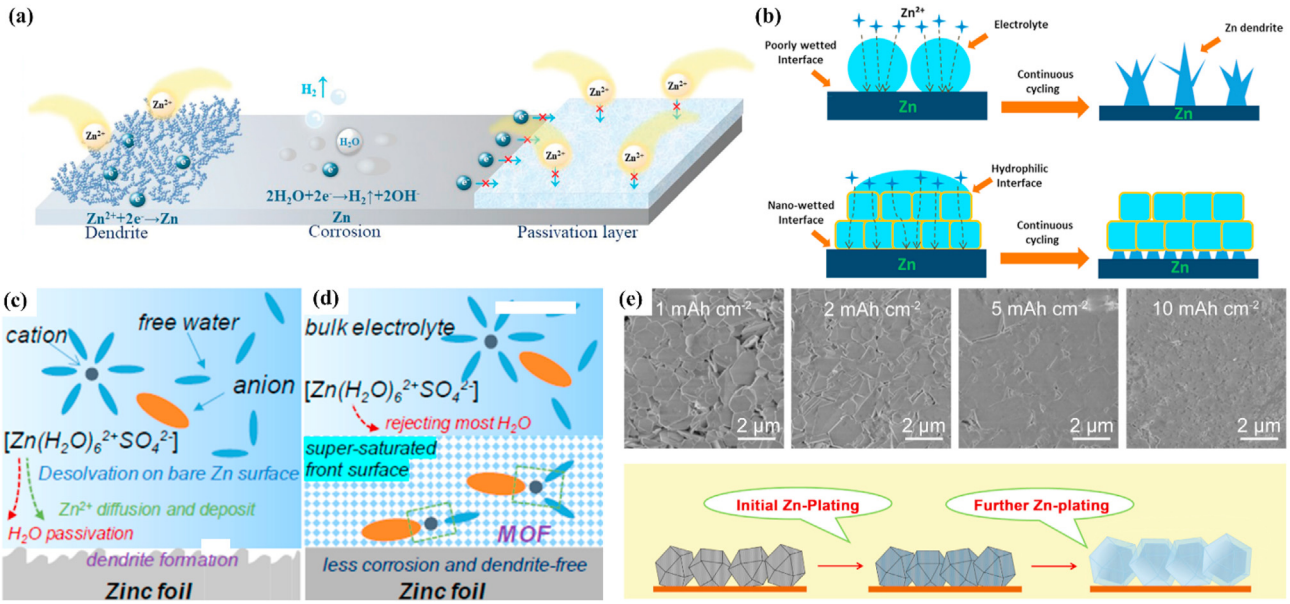


**Fig. 7.** Issues of metal Zn anodes and corresponding coping strategies. (a) Schematic illustration for Zn dendrite, corrosion, and passivation. Reprinted with permission from Ref. [137]. (b) Zinc plating mechanisms on metal zinc electrode without or with artificial SEI film. Reprinted with permission from Ref. [146]. (c–d) Schematic diagram of Zn surface evolution with ZIF-7 constructed super-saturated electrolyte front surface. Reprinted with permission from Ref. [147]. (e) SEM images of zinc deposition on MOF-derived porous anode matrix at a current density of 1.0 mA/cm$^2$ for different deposition capacities and their schematic illustration of the zinc plating. Reprinted with permission from Ref. [148].

have been achieved (Fig. 7b). Recently, an in situ grown ZIF-8 on the Zn anode as the ion modulation layer has been used to regulate $Zn^{2+}$ diffusion behavior, and then ensure uniform Zn deposition and enhance coulombic efficiency [153].

In aqueous Zn-based batteries, dendrite growth, undesired hydrogen evolution, and the formation of $Zn(OH)_x$ in the zinc anode damage the zinc anode, as a result, recently, a 'water-in-salt' strategy has been developed to alleviate the deterioration of the

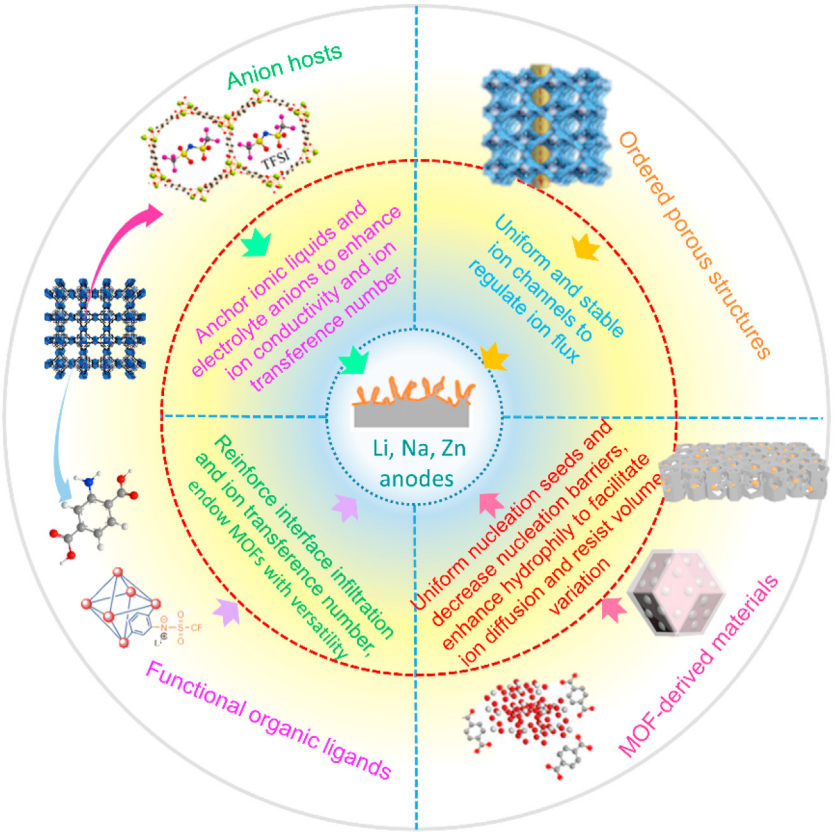


**Fig. 8.** Design principles of MOF-related materials for high stable metal anodes in secondary metal-based batteries.

zinc anode [13,154]. However, the high concentration of salts will increase the cost of batteries. Inspired by the merit of saturated electrolyte systems, Zhou et al. proposed a MOF (ZIF-7) coating layer to homogenize Zn deposition via a concept of super-saturated electrolyte front surface [147]. Raman spectroscopy proved the different diffusion behavior of the highly coordinated ion complexes between MOF channels and bulk electrolytes. The MOF channels would reject the large fraction of water before receiving charge on the Zn surface and then maintain ultra-long reversible cycles in a Zn|Zn symmetric cells (Fig. 7c and d).

*2.3.2. MOF-derived porous anode matrixes*

Carbonized MOF-derived materials have also been used to Zn anode protection recently. Xia and Wang used ZIF-8 as a raw material to fabricate the host for zinc plating/stripping by optimizing the anneal method at 500 °C in insert atmosphere [148]. The resulting material (ZIF-8-500) presents the porous structure accompanying with a homogeneous metal zinc distribution, which is conducive to uniformize zinc plating and increases the high overpotential for hydrogen evolution (Fig. 7e). Recently, a novel MOF-based Zn anode has been prepared by growing MOFs on a selectively oxidized Zn foil surface, and then by the pyrolysis process, which facilitates $Zn^{2+}$ ion diffusion by hydrophilic and porous surfaces [155]. The MOF-based anode exhibits high efficiency and prevents dendrite formation and side reactions during Zn plating/stripping process thereby delivers improved performance.

Based on the excellent hydrophilcity and physicochemical stability, MOF-related materials are viewed as an admirable platform to optimize the interface between aqueous electrolyte and metal zinc anode and construct stable anode scaffold. Recently, suppressing zinc dendrite growth has become an emerging issue, we believe that recent achievements of lithium and sodium anode protection based on MOFs and other materials can enlighten researchers to develop full-fledged zinc anode materials to resolve confronting problems in the rapid development of zinc-based batteries.

## 3. Conclusions and outlook

In this article, some latest important developments of MOF-related materials applied to stabilize metal anodes in secondary metal lithium, sodium, or zinc batteries have been reviewed. On the basis of current research actuality, some following design principles are summarized (Fig. 8):

(1) Suitable pore size MOFs possess favorable ion conductivity, good physicochemical stability, and open homogeneous pore structures, which favor to control uniform metal ion flux. Based on these merits, MOFs can function as additives in liquid electrolyte or fabricate a functional coating layer by mixing them with polymer binders to modify commercial separators and anodes, so as to hamper metal dendrite growth in rechargeable metal-based batteries.
(2) Abundant metal ions in MOFs provide open Lewis acid sites, which can anchor ILs or electrolyte anions, thus leading to the enhancement of ion conductivity and ion transference number. Moreover, by virtue of low melting point, negligible volatility and nonflammability of ILs, IL-incorporated MOFs can serve as electrolytes to realize benign thermal stability and good electrochemical performances of secondary metal-based batteries in a wide temperature range.
(3) Varying functional groups of organic ligands in MOFs provide extra possibilities for reinforcing interface infiltration between electrolyte and metal anode, decreasing electrochemical polarization and enhancing ion transference number, which promote the uniform metal ion plating/stripping behaviors. Hence, functionalized MOFs by polar functional groups and large anionic groups is a promising trend for developing high performance metal anodes.
(4) Uniformly distributed metal ions, carbon atoms, and other heteroatoms in MOFs offer important preconditions for forming conductive 3D host matrixes, which supply their application potentials in dealing with emerging problems in metal-based batteries. Specifically, metal ions in MOF-derived anode matrixes can act as uniformly distributed nucleation seeds in stable 3D hierarchical structures, which is beneficial to reducing nucleation barrier and homogenizing metal deposition process. The flexible carbon scaffolds effectively mitigate the volume change and control metal dendrite growth. Introducing heteroatoms to increase polar sites of MOFs could further improve the interactions with metal ions to realize uniform deposition behavior. Besides, the novel amorphous metal oxide molecular crystal composite materials and single atom array mimic materials derived from MOFs can provide new perspective of applying MOF-based materials to energy storage technology.

In brief, these design principles favor to illuminate the structure–function relationship between MOFs and metal anode stability, which is conducive to developing novel and effective MOF-related materials. To address the presented issues for stable various metal anodes, the further research and application of MOF-related materials can be focused on the following points:

(1) In lithium metal batteries, the researches of MOF-related materials have already proved their availability and good promising, but the high cost of MOFs restricts their further developments in practical applications [156]. Low-cost production of MOF-related materials by economies of scale is necessary. Moreover, the dosage of MOFs in batteries should be seriously considered. Hence, the application of MOFs as electrolyte additives, thin separator coating layers and artificial SEIs as well as electrolyte fillers should be more economical and practical in the upcoming commercialization.
(2) It can be clearly seen from the aforementioned progresses that the application investigations on MOF-related materials in sodium and zinc metal batteries are very sporadic, signifying that some effective and feasible technical strategies for stable lithium metal batteries should be energetically explored to surmount the emerging problems of unstable sodium and zinc anodes. In particular, most MOFs present poor stability in aqueous acid/base solutions, which should be carefully considered in designing stable zinc metal batteries with MOFs [156]. In addition, the development of newly designed MOFs with high stability is also a worthwhile research direction.
(3) Severe challenges of large volume change, extremely high reactivity, unstable interface, and barbaric K dendrite growth in metal K anode hampered the further development of potassium-ion batteries although many merits such as high theoretical specific capacity (687 mAh/g), low electrochemical potential (−2.93 V vs. SHE), and high abundance make the metal K promising [157,158]. Some universal strategies by host structure, interfacial engineering, alloying, and electrolyte designing have already gained some progresses in solving the issues of K metal anodes [159−161]. Recently, MOFs as $K^+$ hosts show high performance [162,163]; however, the research of MOF-related materials in K anode

protection is still absent, which is promising and deserves to be carried out.

In a word, seeking and preparing some designable and controllable MOFs can provide more possibilities to develop advanced energy storage technologies. We hope that the expounded structure–function relationship and the referential opinions can guide better design and application of MOFs for a better future.

## Declaration of competing interest

The authors declare that they have no known competing financial interests or personal relationships that could have appeared to influence the work reported in this paper.

## Acknowledgments

This work was financially supported by the National Natural Science Foundation of China (21871077, 21671054, 21771052, 22071042, 21902044, 22001057), the Program for Innovation Teams in Science and Technology in Universities of Henan Province (20IRTSTHN004), the Major Project of Science and Technology of Henan Province Office of Education (202102310224), the Program of First-Class Discipline Cultivation Project of Henan University (2019YLZDYJ02).

## References

[1] J.-Y. Hwang, S.-T. Myung, Y.-K. Sun, Chem. Soc. Rev. 46 (2017) 3529–3614.
[2] H.B. Wu, X.W. Lou, Sci. Adv. 3 (2017), eaap9252.
[3] X. Zhou, H. Xie, X. He, Z. Zhao, Q. Ma, M. Cai, H. Yin, Energy Environ. Mater. 3 (2020) 166.
[4] C. Delmas, Adv. Energy Mater. 8 (2018), 1703137.
[5] M. Zhu, J. Wu, Y. Wang, M. Song, L. Long, S.H. Siyal, X. Yang, G. Sui, J. Energy Chem. 37 (2018) 126–142.
[6] G. Fang, J. Zhou, A. Pan, S. Liang, ACS Energy Lett. 3 (2018) 2480–2501.
[7] X.-B. Cheng, M.-Q. Zhao, C. Chen, A. Pentecost, K. Maleski, T. Mathis, X.-Q. Zhang, Q. Zhang, J. Jiang, Y. Gogotsi, Nat. Commun. 8 (2017) 336.
[8] J. Yu, R. Ran, Y. Zhong, W. Zhou, M. Ni, Z. Shao, Energy Environ. Mater. 3 (2020) 121.
[9] Q. He, B. Yu, Z. Li, Y. Zhao, Energy Environ. Mater. 2 (2019) 264.
[10] F. Wu, Y.X. Yuan, X.B. Cheng, Y. Bai, Y. Li, C. Wu, Q. Zhang, Energy Storage Mater. 15 (2018) 148–170.
[11] Z.W. Seh, Y. Sun, Q. Zhang, Y. Cui, Chem. Soc. Rev. 45 (2016) 5605–5634.
[12] L. Chen, L.L. Shaw, J. Power Sources 267 (2014) 770–783.
[13] F. Wang, O. Borodin, T. Gao, X. Fan, W. Sun, F. Han, A. Faraone, J.A. Dura, K. Xu, C. Wang, Nat. Mater. 17 (2018) 543–549.
[14] L. Fan, X. Li, Nanomater. Energy 53 (2018) 630–642.
[15] W. Lu, C. Xie, H. Zhang, X. Li, ChemSusChem 11 (2018) 3996–4006.
[16] X. Cheng, Q. Zhang, Prog. Chem. 30 (2018) 51–72.
[17] M. Ghosh, V. Vijayakumar, S. Kurungot, Energy Technol. 7 (2019), 1900442.
[18] A. Jana, D.R. Ely, R.E. García, J. Power Sources 275 (2015) 912–921.
[19] W. Lu, Y. Han, F. Xiao, J. Zhou, P. Qi, W. Bo, Coord. Chem. Rev. 307 (2015) 361–381.
[20] D. Zou, D. Liu, J. Zhang, Energy Environ. Mater. 1 (2018) 209.
[21] U. Ryu, S. Jee, P.C. Rao, J. Shin, C. Ko, M. Yoon, K.S. Park, K.M. Choi, Coord. Chem. Rev. 426 (2021) 213544–213616.
[22] Z. Yang, Z. Song, L. Xia, S. Qian, N. Cheng, S. Lawes, X. Sun, Energy Storage Mater. 2 (2015) 35–62.
[23] H. Yang, W. Cui, Y. Han, B. Wang, Chin. Chem. Lett. 39 (2018) 842–844.
[24] Z. Bai, Y. Zhang, Y. Zhang, C. Guo, B. Tang, D. Sun, J. Mater. Chem. 3 (2015) 5266–5269.
[25] X. Han, W.-M. Chen, X. Han, Y.-Z. Tan, D. Sun, J. Mater. Chem. 4 (2016) 13040–13045.
[26] L. Zhang, H. Liu, W. Shi, P. Cheng, Coord. Chem. Rev. 388 (2019) 293–309.
[27] Y. Du, X. Gao, S. Li, L. Wang, B. Wang, Chin. Chem. Lett. 31 (2020) 609–616.
[28] M.R. Palacín, G.A. De, Science 351 (2016), 1253292.
[29] J. Janek, W.G. Zeier, Energy 500 (2016) 300.
[30] G. Zheng, S.W. Lee, Z. Liang, H.-W. Lee, K. Yan, H. Yao, H. Wang, W. Li, S. Chu, Y. Cui, Nat. Nanotechnol. 9 (2014) 618.
[31] S. Zheng, H. Xue, H. Pang, Coord. Chem. Rev. 373 (2018) 2–21.
[32] D. Zhou, D. Shanmukaraj, A. Tkacheva, M. Armand, G. Wang, Inside Chem. 5 (2019) 2326–2352.
[33] C. Fang, Y. Wang, W. Liu, R. Guo, J. Xie, Mater. Today Energy 17 (2020) 100415–100421.
[34] H. Zhang, G.G. Eshetu, X. Judez, C. Li, L.M. Rodriguez-Martínez, M. Armand, Angew. Chem. Int. Ed. 57 (2018) 15002–15027.
[35] X.Q. Zhang, X.B. Cheng, X. Chen, C. Yan, Q. Zhang, Adv. Funct. Mater. 27 (2017), 1605989.
[36] K. Fujie, H. Kitagawa, Coord. Chem. Rev. 307 (2016) 382–390.
[37] K. Fujie, R. Ikeda, K. Otsubo, T. Yamada, H. Kitagawa, Chem. Mater. 27 (2015) 7355–7361.
[38] Z. Wang, R. Tan, H. Wang, L. Yang, J. Hu, H. Chen, F. Pan, Adv. Mater. 30 (2018), 1704436.
[39] K. Wang, L. Yang, Z. Wang, Y. Zhao, F. Pan, Chem. Commun. 54 (2018) 13060–13063.
[40] W. Xu, J. Wang, F. Ding, X. Chen, E. Nasybulin, Y. Zhang, J.-G. Zhang, Energy Environ. Sci. 7 (2014) 513–537.
[41] N. Chen, Y. Li, Y. Dai, W. Qu, Y. Xing, Y. Ye, Z. Wen, C. Guo, F. Wu, R.J. Chen, J. Mater. Chem. 7 (2019) 9530–9536.
[42] L. Sun, S.S. Park, D. Sheberla, M.J. Dincă, J. Am. Chem. Soc. 138 (2016) 14772–14782.
[43] S.S. Park, Y. Tulchinsky, M. J Dincă, J. Am. Chem. Soc. 139 (2017) 13260–13263.
[44] Z. Wang, Z. Wang, L. Yang, H. Wang, Y. Song, H. Lei, Y. Kai, J. Hu, H. Chen, P. Feng, Nanomater. Energy 49 (2018) 580–587.
[45] J. Qian, Y. Li, M. Zhang, R. Luo, F. Wang, Y. Ye, Y. Xing, W. Li, W. Qu, L. Wang, Nanomater. Energy 60 (2019) 866–874.
[46] L. Fan, Z. Guo, Y. Zhang, X. Wu, C. Zhao, X. Sun, G. Yang, Y. Feng, N. Zhang, J. Mater. Chem. 8 (2020) 251–258.
[47] Z.-J. Zheng, Q. Su, Q. Zhang, X.-C. Hu, Y.-X. Yin, R. Wen, H. Ye, Z.-B. Wang, Y.-G. Guo, Nanomater. Energy 64 (2019) 103910–103917.
[48] G. Wang, P. He, L.Z. Fan, Adv. Funct. Mater. (2020), 2007198.
[49] Y. Lu, Z. Tu, L.A. Archer, Nat. Mater. 13 (2014) 961.
[50] K. Park, J.B. Goodenough, Adv. Energy Mater. 7 (2017), 1700732.
[51] H. Ye, Y.-X. Yin, S.-F. Zhang, Y. Shi, L. Liu, X.-X. Zeng, R. Wen, Y.-G. Guo, L.-J. Wan, Nanomater. Energy 36 (2017) 411–417.
[52] F. Chu, J. Hu, C. Wu, Z. Yao, J. Tian, Z. Li, C. Li, ACS Appl. Mater. Interfaces 11 (2018) 3869–3879.
[53] Y. He, Z. Chang, S. Wu, Y. Qiao, S. Bai, K. Jiang, P. He, H. Zhou, Adv. Energy Mater. 8 (2018), 1802130.
[54] J. Hu, J. Tian, C. Li, ACS Appl. Mater. Interfaces 9 (2017) 11615–11625.
[55] X.-X. Zeng, Y.-X. Yin, N.-W. Li, W.-C. Du, Y.-G. Guo, L.-J. Wan, J. Am. Chem. Soc. 138 (2016) 15825–15828.
[56] X. Han, Y. Gong, K.K. Fu, X. He, G.T. Hitz, J. Dai, A. Pearse, B. Liu, H. Wang, G. Rubloff, Nat. Mater. 16 (2017) 572.
[57] W. Yao, L. Liu, X.S. Wu, C. Qin, H. Xie, Z.M. Su, ACS Appl. Mater. Interfaces 10 (2018) 35911–35918.
[58] N. Yan, W. Zhang, J. Shi, Y. Liu, H. Cui, Mater. Lett. 229 (2018) 198–201.
[59] J.C. Ye, J.J. Chen, R.M. Yuan, D.R. Deng, M.S. Zheng, L. Cronin, Q.F. Dong, J. Am. Chem. Soc. 140 (2018) 3134–3138.
[60] N. Deng, W. Kang, Y. Liu, J. Ju, D. Wu, L. Li, B.S. Hassan, B. Cheng, J. Power Sources 331 (2016) 132–155.
[61] N. Deng, L. Wang, Y. Feng, M. Liu, Q. Li, G. Wang, L. Zhang, W. Kang, B. Cheng, Y. Liu, Chem. Eng. J. 338 (2020) 124241–124254.
[62] S. Bai, X. Liu, K. Zhu, S. Wu, H. Zhou, Nat. Energy 1 (2016), 16094.
[63] Y. Zhang, Z. Gao, N. Song, J. He, X. Li, Mater. Today Energy 9 (2018) 319–335.
[64] C. Qi, L. Xu, J. Wang, H. Li, C. Zhao, L. Wang, T. Liu, ACS Sustain. Chem. Eng. 8 (2020) 12968–12975.
[65] W. Tang, S. Tang, C. Zhang, Q. Ma, Q. Xiang, Y.W. Yang, J. Luo, Adv. Energy Mater. 8 (2018), 1800866.
[66] Q. Han, S. Wang, Z. Jiang, X. Hu, H. Wang, ACS Appl. Mater. Interfaces 12 (2020) 20514–20521.
[67] Y. Li, S. Lin, D. Wang, T. Gao, J. Song, P. Zhou, Z. Xu, Z. Yang, N. Xiao, S. Guo, Adv. Mater. 32 (2020), 1906722.
[68] X. Lu, H. Wu, D. Kong, X. Li, L. Shen, Y. Lu, ACS Mater. Lett. 2 (2020) 1435–1441.
[69] J.-F. Wu, X.J. Guo, J. Mater. Chem. 7 (2019) 2653–2659.
[70] Y. Xia, N. Xu, L. Du, Y. Cheng, S. Lei, S. Li, X. Liao, W. Shi, L. Xu, L. Mai, ACS Appl. Mater. Interfaces 12 (2020) 22930–22938.
[71] D.R. MacFarlane, M. Forsyth, P.C. Howlett, M. Kar, S. Passerini, J.M. Pringle, H. Ohno, M. Watanabe, F. Yan, W. Zheng, Nat. Rev. Mater. 1 (2016), 15005.
[72] K. Shikinaka, N. Taki, K. Kaneda, Y. Tominaga, Chem. Commun. 53 (2017) 613–616.
[73] D.-D. Han, Z.-Y. Wang, G.-L. Pan, X.-P. Gao, ACS Appl. Mater. Interfaces 11 (2019) 18427–18435.
[74] F. Croce, L. Settimi, B. Scrosati, Electrochem. Commun. 8 (2006) 364–368.
[75] S. Bai, Y. Sun, J. Yi, Y. He, Y. Qiao, H. Zhou, Joule 2 (2018) 2117–2132.
[76] L. Shen, H.B. Wu, F. Liu, J.L. Brosmer, G. Shen, X. Wang, J.I. Zink, Q. Xiao, M. Cai, G. Wang, Y. Lu, B. Dunn, Adv. Mater. 30 (2018), 1707476.
[77] S. Yuan, J.L. Bao, C. Li, Y. Xia, D.G. Truhlar, Y. Wang, ACS Appl. Mater. Interfaces 11 (2019) 10616–10623.
[78] D.E. Mathew, S. Gopi, M. Kathiresan, A.M. Stephan, S. Thomas, Electrochim. Acta 319 (2019) 189–200.
[79] H. Huo, B. Wu, T. Zhang, X. Zheng, L. Ge, T. Xu, X. Guo, X. Sun, Energy Storage Mater. 18 (2019) 59–67.
[80] L. Shen, H.B. Wu, F. Liu, C. Zhang, S. Ma, Z. Le, Y. Lu, Nanoscale Horiz 4 (2019) 705–711.
[81] H. Wang, Q. Wang, X. Cao, Y. He, K. Wu, J. Yang, H. Zhou, W. Liu, X. Sun, Adv. Mater. 32 (2020), 2001259.

[82] HyunSeok Jeong, S.C. Hong, S.-Y. Lee, J. Membr. Sci. 364 (2010) 177–182.
[83] Y. Guan, A. Wang, S. Liu, Q. Li, W. Wang, Y.J. Huang, J. Alloys Compd. 765 (2018) 544–550.
[84] H. Shao, W. Wang, Z. Hao, A. Wang, X. Chen, Y. Huang, J. Power Sources 378 (2018) 537–545.
[85] X. Zhu, X. Jiang, X. Ai, H. Yang, Y.J. Cao, J. Membr. Sci. 4 (2016) 97–103.
[86] M. Waqas, S. Ali, W. Lv, D. Chen, B. Boateng, W. He, Adv. Mater. Interfaces 6 (2019), 1801330.
[87] Z. Zhang, Y. Lai, Z. Zhang, K. Zhang, J. Li, Electrochim. Acta 129 (2014) 55–61.
[88] Z. Tu, Y. Kambe, Y. Lu, L.A. Archer, Adv. Energy Mater. 4 (2014), 1300654.
[89] W. Luo, L. Zhou, K. Fu, Z. Yang, J. Wan, M. Manno, Y. Yao, H. Zhu, B. Yang, L. Hu, Nano Lett. 15 (2015) 6149–6154.
[90] Z. Tu, M.J. Zachman, S. Choudhury, S. Wei, L. Ma, Y. Yang, L.F. Kourkoutis, L.A. Archer, Adv. Energy Mater. 7 (2017), 1602367.
[91] W. Liu, Y. Mi, Z. Weng, Y. Zhong, Z. Wu, H. Wang, Chem. Sci. 8 (2017) 4285–4291.
[92] K. Yang, L. Zhong, Y. Mo, R. Wen, M. Xiao, D. Han, S. Wang, Y. Meng, ACS Appl. Energy Mater. 1 (2018) 2555–2564.
[93] K. Yang, L. Zhong, R. Guan, M. Xiao, D. Han, S. Wang, Y. Meng, Appl. Surf. Sci. 441 (2018) 914–922.
[94] L. Ma, P. Nath, Z. Tu, M. Tikekar, L.A. Archer, Chem. Mater. 28 (2016) 5147–5154.
[95] X. Yu, J. Joseph, A. Manthiram, Mater. Horiz. 3 (2016) 314–319.
[96] S.H. Kim, J.S. Yeon, R. Kim, K.M. Choi, H.S. Park, J. Mater. Chem. 6 (2018) 24971–24978.
[97] F. Zhu, H. Bao, X. Wu, Y. Tao, C. Qin, Z. Su, Z. Kang, ACS Appl. Mater. Interfaces 11 (2019) 43206–43213.
[98] Q. Zhang, B. Liu, J. Wang, Q. Li, D. Li, S. Guo, Y. Xiao, Q. Zeng, W. He, M. Zheng, Y. Ma, S. Huang, ACS Energy Lett. 5 (2020) 2919–2926.
[99] P. Chiochan, X. Yu, M. Sawangphruk, A. Manthiram, Adv. Energy Mater. 10 (2020), 2001285.
[100] K. Deng, Q. Zeng, D. Wang, Z. Liu, Z. Qiu, Y. Zhang, M. Xiao, Y. Meng, J. Mater. Chem. 8 (2020) 1557–1577.
[101] L. Porcarelli, A.S. Shaplov, F. Bella, J.R. Nair, D. Mecerreyes, C. Gerbaldi, ACS Energy Lett. 1 (2016) 678–682.
[102] Q. Zhang, D. Li, J. Wang, S. Guo, W. Zhang, D. Chen, Q. Li, X. Rui, L. Gan, S. Huang, Nanoscale 12 (2020) 6976–6982.
[103] C.-P. Yang, Y.-X. Yin, S.-F. Zhang, N.-W. Li, Y.-G. Guo, Nat. Commun. 6 (2015), 8058.
[104] R. Zhang, X.R. Chen, X. Chen, X.B. Cheng, X.Q. Zhang, C. Yan, Q. Zhang, Angew. Chem. Int. Ed. 56 (2017) 7764–7768.
[105] K. Yan, Z. Lu, H.-W. Lee, F. Xiong, P.-C. Hsu, Y. Li, J. Zhao, S. Chu, Y. Cui, Nat. Energy 1 (2016) 16010.
[106] C. Jin, O. Sheng, J. Luo, H. Yuan, C. Fang, W. Zhang, H. Huang, Y. Gan, Y. Xia, C. Liang, Nanomater. Energy 37 (2017) 177–186.
[107] L.-L. Lu, J. Ge, J.-N. Yang, S.-M. Chen, H.-B. Yao, F. Zhou, S.-H. Yu, Nano Lett. 16 (2016) 4431–4437.
[108] F. Wang, H.-Y. Zhuo, X. Han, W.-M. Chen, D. Sun, J. Mater. Chem. 5 (2017) 22964–22969.
[109] Y. Chu, L. Guo, B. Xi, Z. Feng, F. Wu, Y. Lin, J. Liu, D. Sun, J. Feng, Y. Qian, Adv. Mater. 30 (2018), 1704244.
[110] X. Han, L. Sun, F. Wang, D. Sun, J. Mater. Chem. 6 (2018) 18891–18897.
[111] F. Wu, S. Zhang, B. Xi, Z. Feng, D. Sun, X. Ma, J. Zhang, J. Feng, S. Xiong, Adv. Energy Mater. 8 (2018), 1703242.
[112] M. Zhu, B. Li, S. Li, Z. Du, Y. Gong, S. Yang, Adv. Energy Mater. 8 (2018), 1703505.
[113] D. Yin, G. Huang, S. Wang, D. Yuan, X. Wang, Q. Li, Q. Sun, H. Xue, L. Wang, J. Ming, J. Mater. Chem. 8 (2020) 1425–1431.
[114] Y. Zhong, F. Lin, M. Wang, Y. Zhang, Q. Ma, J. Lin, Z. Feng, H. Wang, Adv. Funct. Mater. 30 (2020), 1907579.
[115] L. Wang, X. Zhu, Y. Guan, J. Zhang, F. Ai, W. Zhang, Y. Xiang, S. Vijayan, G. Li, Y. Huang, Energy Storage Mater. 11 (2018) 191–196.
[116] S.J. Zhang, J.H. You, J.D. Chen, Y.Y. Hu, C.W. Wang, Q. Liu, Y.Y. Li, Y. Zhou, J.T. Li, J. Swiatowska, L. Huang, S.G. Sun, ACS Appl. Mater. Interfaces 11 (2019) 47939–47947.
[117] L. Wei, L. Li, T. Zhao, N. Zhang, Y. Zhao, F. Wu, R. Chen, Nanoscale 12 (2020) 9416–9422.
[118] S. Fu, L. Wang, T. Zhao, L. Li, F. Wu, R. Chen, ChemElectroChem 7 (2020) 2159–2164.
[119] J. Xiao, H. Liu, J. Huang, Y. Lu, L. Zhang, Appl. Surf. Sci. 526 (2020) 146746–146758.
[120] K. Wu, B. Zhao, C. Yang, Q. Wang, W. Liu, H. Zhou, J. Energy Chem. 43 (2020) 16–23.
[121] M. Zhu, J. Zhang, Y. Ma, Y. Nan, S. Li, Carbon 168 (2020) 633–639.
[122] T.S. Wang, X. Liu, Y. Wang, L.Z. Fan, Adv. Funct. Mater. (2020), 2001973.
[123] M. Zhu, S. Li, B. Li, Y. Gong, Z. Du, S. Yang, Sci. Adv. 5 (2019), eaau6264.
[124] L. Jing, G. Lian, F. Niu, J. Yang, Q. Wang, D. Cui, C.-P. Wong, X. Liu, Nanomater. Energy 51 (2018) 546–555.
[125] C. Zhao, C. Yu, B. Qiu, S. Zhou, M. Zhang, H. Huang, B. Wang, J. Zhao, X. Sun, J. Qiu, Adv. Mater. 30 (2018), 1702486.
[126] C. Yang, J. Xiong, X. Ou, C.-F. Wu, X. Xiong, J.-H. Wang, K. Huang, M. Liu, Mater. Today Energy 8 (2018) 37–44.
[127] X. Bi, X. Ren, Z. Huang, M. Yu, E. Kreidler, Y. Wu, Chem. Commun. 51 (2015) 7665–7668.
[128] S. Wei, S. Choudhury, J. Xu, P. Nath, Z. Tu, L.A. Archer, Adv. Mater. 29 (2017), 1605512.
[129] S. Choudhury, S. Wei, Y. Ozhabes, D. Gunceler, M.J. Zachman, Z. Tu, J.H. Shin, P. Nath, A. Agrawal, L.F. Kourkoutis, Nat. Commun. 8 (2017) 898.
[130] J. Sun, C. Guo, Y. Cai, J. Li, X. Sun, W. Shi, S. Ai, C. Chen, F. Jiang, Electrochim. Acta 309 (2019) 18–24.
[131] C. Chen, T. Li, H. Tian, Y. Zou, J. Sun, J. Mater. Chem. 7 (2019) 18451–18457.
[132] J. Sun, M. Zhang, P. Ju, Y. Hu, X. Chen, W. Wang, C. Chen, Energy Technol. 8 (2020), 1901250.
[133] G. Abbas, S.M. Alay-e-Abbas, A. Laref, Y. Li, W.X. Zhang, Mater. Today Energy 17 (2020) 100486–100493.
[134] N. Mubarak, M. Ihsan-Ul-Haq, H. Huang, J. Cui, S. Yao, A. Susca, J. Wu, M. Wang, X. Zhang, B. Huang, J.-K. Kim, J. Mater. Chem. 8 (2020) 10269–10282.
[135] Y. Xie, J. Hu, Z. Han, T. Wang, J. Zheng, L. Gan, Y. Lai, Z. Zhang, Energy Storage Mater. 30 (2020) 1–8.
[136] Y. Li, J. Fu, C. Zhong, T. Wu, Z. Chen, W. Hu, K. Amine, J. Lu, Adv. Energy Mater. 9 (2019), 1802605.
[137] B. Tang, L. Shan, S. Liang, J. Zhou, Energy Environ. Sci. 12 (2019) 3288–3304.
[138] D. Chao, W. Zhou, F. Xie, C. Ye, S.Z. Qiao, Sci. Adv. 6 (2020), eaba4098.
[139] D. Chao, C. Ye, F. Xie, W. Zhou, Q. Zhang, Q. Gu, K. Davey, L. Gu, S.Z. Qiao, Adv. Mater. 32 (2020), e2001894.
[140] M. Song, H. Tan, D. Chao, H.J. Fan, Adv. Funct. Mater. 28 (2018), 1802564.
[141] A.C. Khor, P.K. Leung, M.R. Mohamed, C. Flox, A. Shah, Mater. Today Energy 8 (2018) 80–108.
[142] D. Chao, W. Zhou, C. Ye, Q. Zhang, Y. Chen, L. Gu, K. Davey, S.Z. Qiao, Angew Chem. Int. Ed. Engl. 58 (2019) 7823–7828.
[143] C.-C. Chang, Y.-C. Lee, H.-J. Liao, Y.-T. Kao, J.-Y. An, D.-Y. Wang, ACS Sustain. Chem. Eng. 7 (2018) 2860–2866.
[144] Z. Wang, H. Li, Z. Tang, Z. Liu, Z. Ruan, L. Ma, Q. Yang, D. Wang, C. Zhi, Adv. Funct. Mater. 28 (2018), 1804560.
[145] J. Huang, Z. Guo, Y. Ma, D. Bin, Y. Wang, Y. Xia, Small Methods 3 (2019), 1800272.
[146] M. Liu, L. Yang, H. Liu, A. Amine, Q. Zhao, Y. Song, J. Yang, K. Wang, F. Pan, ACS Appl. Mater. Interfaces 11 (2019) 32046–32051.
[147] H. Yang, Z. Chang, Y. Qiao, H. Deng, X. Mu, P. He, H. Zhou, Angew Chem. Int. Ed. Engl. 59 (2020) 9377–9381.
[148] Z. Wang, J. Huang, Z. Guo, X. Dong, Y. Liu, Y. Wang, Y. Xia, Joule 3 (2019) 1289–1300.
[149] D. Chao, S.Z. Qiao, Joule 4 (2020) 1839–1851.
[150] B.S. Lee, S. Cui, X. Xing, H. Liu, X. Yue, V. Petrova, H.D. Lim, R. Chen, P. Liu, ACS Appl. Mater. Interfaces 10 (2018) 38928–38935.
[151] J. Zheng, Q. Zhao, T. Tang, J. Yin, C.D. Quilty, G.D. Renderos, X. Liu, Y. Deng, L. Wang, D.C. Bock, Science 366 (2019) 645–648.
[152] Z. Wang, J. Hu, L. Han, Z. Wang, H. Wang, Q. Zhao, J. Liu, F. Pan, Nanomater. Energy 56 (2019) 92–99.
[153] X. Liu, F. Yang, W. Xu, Y. Zeng, J. He, X. Lu, Adv. Sci. 7 (2020), 2002173.
[154] L. Suo, O. Borodin, T. Gao, M. Olguin, J. Ho, X. Fan, C. Luo, C. Wang, K. Xu, Science 350 (2015) 938–943.
[155] R. Yuksel, O. Buyukcakir, W.K. Seong, R.S. Ruoff, Adv. Energy Mater. 10 (2020), 1904251.
[156] U. Ryu, S. Jee, P.C. Rao, J. Shin, C. K, M. Yoon, K.S. Park, K.M. Cho, Acc. Chem. Res. 426 (2021) 213544–213616.
[157] C. Wei, Y. Tao, H. Fei, Y. An, Y. Tian, J. Feng, Y. Qian, Energy Storage Mater. 30 (2020) 206–227.
[158] P. Liu, D. Mitlin, Acc. Chem. Res. 53 (2020) 1161–1175.
[159] L. Xue, H. Gao, W. Zhou, S. Xin, K. Park, Y. Li, J.B. Goodenough, Adv. Mater. 28 (2016) 9608–9612.
[160] N. Xiao, W.D. McCulloch, Y. Wu, J. Am. Chem. Soc. 139 (2017) 9475–9478.
[161] P. Liu, Y. Wang, Q. Gu, J. Nanda, J. Watt, D. Mitlin, Adv. Mater. 32 (2020), e1906735.
[162] P. Xiao, S. Li, C. Yu, Y. Wang, Y. Xu, ACS Nano 14 (2020) 10210–10218.
[163] Q. Deng, Z. Luo, H. Liu, Y. Zhou, C. Zhou, R. Yang, L. Wang, Y. Yan, Y. Xu, Ionics 26 (2020) 5565–5573.